

Hyperfine-induced decoherence in triangular spin-cluster qubits

Filippo Troiani,¹ Dimitrije Stepanenko,² and Daniel Loss²

¹*S3, Istituto Nanoscienze-CNR, via G. Campi 213/A, I-41100 Modena, Italy*

²*Department of Physics, University of Basel, Klingbergstrasse 82, CH-4056 Basel, Switzerland*

(Received 25 May 2012; published 17 October 2012)

We theoretically investigate hyperfine-induced decoherence in a triangular spin cluster for different qubit encodings. Electrically controllable eigenstates of spin chirality (C_z) show no appreciable decoherence up to $10^2 \mu\text{s}$, while a complete decoherence is estimated for the eigenstates of the total-spin projection (S_z) and of the partial spin sum (S_{12}) after $10 \mu\text{s}$. The robustness of chirality is due to its decoupling from both the total- and individual-spin components in the cluster. This results in a suppression of the effective interaction between C_z and the nuclear-spin bath. We finally estimate the reduction of the decoherence time scale for C_z , resulting from possible hyperfine contact terms or from the misalignment of the magnetic field.

DOI: [10.1103/PhysRevB.86.161409](https://doi.org/10.1103/PhysRevB.86.161409)

PACS number(s): 03.65.Yz, 03.67.Lx, 75.50.Xx

Introduction. Molecular nanomagnets represent a varied class of spin clusters, whose physical properties can be extensively engineered by chemical synthesis.¹ This makes them a potential alternative to other spin systems² for the implementation of spin-cluster qubits.^{3–5} While most of the attention has been so far focused on the use of the total-spin projection (S_z) as a computational degree of freedom (DOF), it has been recently realized that alternative encodings would enable the use of electric—rather than magnetic—fields for the qubit manipulation.⁶ In particular, transitions between states of opposite spin chirality [$C_z = (4/\sqrt{3})\mathbf{s}_1 \cdot \mathbf{s}_2 \times \mathbf{s}_3$] can be induced in antiferromagnetic triangles with Dzyaloshinskii-Moriya interaction. Spin-electric coupling constants compatible with ns gating times τ_g have been predicted by effective models^{6,7} and microscopic *ab initio* calculations,⁸ and might be possibly enhanced by suitable chemical substitutions.⁹

In order to assess the suitability of spin chirality for applications in quantum-information processing, its τ_g has to be contrasted with a characteristic decoherence time τ_d . At low temperatures, quantum coherence in molecular nanomagnets is limited by the coupling to the nuclear-spin environment, with typical values of τ_d in the microsecond range.^{10–12} All the existing literature is, however, concerned with linear superpositions of different S_z eigenstates. Here we theoretically investigate the dependence of hyperfine-induced decoherence on the qubit encoding within a prototypical spin-cluster qubit, consisting of an antiferromagnetic spin triangle. In particular, we consider three different DOFs, namely, S_z , C_z , and the partial spin sum S_{12} ($\mathbf{S}_{12} = \mathbf{s}_1 + \mathbf{s}_2$), whose value—as that of C_z —can be controlled through spin-electric coupling. Since the optimal candidate system has not been identified yet, we refer here to a prototypical molecular spin-cluster qubit, with a typical electron-spin Hamiltonian¹³ and bath of nuclear spins.¹⁴

Qubit encodings in the spin triangle. We consider a triangle of $1/2$ spins, with a dominant antiferromagnetic coupling and Zeeman interaction:

$$H_0 = J \sum_{i=1}^3 \mathbf{s}_i \cdot \mathbf{s}_{i+1} + g\mu_B \mathbf{B} \cdot \mathbf{S}. \quad (1)$$

An additional term H_1 determines the expression of the lowest eigenstates $|0\rangle$ and $|1\rangle$, belonging to the ground state $S = 1/2$

quadruplet. As discussed in the following, the robustness of the spin-cluster qubit with respect to hyperfine-induced decoherence strongly depends on the distinguishability between $|0\rangle$ and $|1\rangle$ in terms not only of total-spin orientation, but also of spin texture. Hereafter, we thus discuss these features in some detail in two relevant cases:

$$H_1^{C_z} = \frac{\Delta}{\sqrt{3}} \hat{\mathbf{z}} \cdot \sum_{i=1}^3 \mathbf{s}_i \times \mathbf{s}_{i+1}, \quad (2)$$

$$H_1^{S_{12}} = (J_{12} - J)\mathbf{s}_1 \cdot \mathbf{s}_2. \quad (3)$$

The term $H_1^{C_z}$ accounts for the Dzyaloshinskii-Moriya interaction.¹³ For an electron-spin Hamiltonian $H_e = H_0 + H_1^{C_z}$, the four lowest eigenstates can be labeled after the value of the spin chirality C_z , and the Dzyaloshinskii-Moriya term can be rephrased as $H_1^{C_z} = \Delta C_z S_z$.⁶ If the magnetic field is oriented parallel to the principal axis (z) of the molecule, the eigenstates $|C_z, S_z\rangle$ read $|\pm 1, +1/2\rangle = (|\downarrow\uparrow\uparrow\rangle + e^{\pm i2\pi/3}|\uparrow\downarrow\uparrow\rangle + e^{\mp i2\pi/3}|\uparrow\uparrow\downarrow\rangle)/\sqrt{3}$ and $|\pm 1, -1/2\rangle = \sigma_x^1 \sigma_x^2 \sigma_x^3 |\pm 1, +1/2\rangle$, where σ_x^i is the Pauli operator acting on \mathbf{s}_i . Both S_z and C_z commute with H_e , which makes them suitable as computational DOFs. In the first case, the logical states are

$$|0\rangle_{S_z} = |S_z = -1/2; C_z = +1\rangle,$$

$$|1\rangle_{S_z} = |S_z = +1/2; C_z = +1\rangle,$$

with spin expectation values [Fig. 1(a)]

$$\langle 1|s_{z,i}|1\rangle_{S_z} = -\langle 0|s_{z,i}|0\rangle_{S_z} = 1/6. \quad (4)$$

If the computational DOF is identified with spin chirality, the logical states are instead

$$|0\rangle_{C_z} = |C_z = +1; S_z = -1/2\rangle,$$

$$|1\rangle_{C_z} = |C_z = -1; S_z = -1/2\rangle,$$

and the expectation values of the three spins are independent on the qubit state [Fig. 1(a)],

$$\langle 1|s_{z,i}|1\rangle_{C_z} = \langle 0|s_{z,i}|0\rangle_{C_z} = -1/6. \quad (5)$$

As a result, $|0\rangle_{C_z}$ and $|1\rangle_{C_z}$ are indistinguishable in terms of total-spin projection and spin texture: They thus span an approximately decoherence-free subspace^{15–17} (see below). Such a condition is, however, not general. In fact, if the

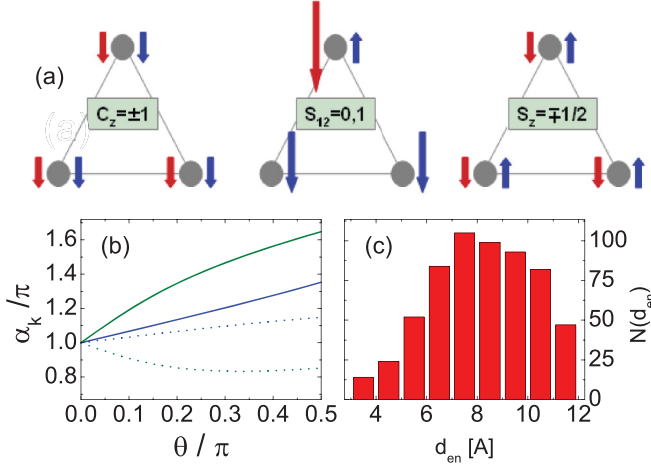


FIG. 1. (Color online) (a) Schematics of the local spin projections $\langle s_{z,i} \rangle$ in the spin triangle, corresponding to the $|0\rangle$ (red) and $|1\rangle$ (blue) states in the three considered qubit encodings. The logical states of the chirality qubit (C_z , left) have identical expectation values $\langle s_{z,i} \rangle$; this is not the case for the other two encodings (S_{12} and S_z). (b) Angle α_k between the vector $\langle \mathbf{S} \rangle$ and $\hat{\mathbf{z}}$ for the eigenstates $|0\rangle_{C_z}^\theta$ (blue) and $|1\rangle_{C_z}^\theta$ (green), for $\Delta/g\mu_B = 0.5$ (solid lines) and 2.0 (dotted). (c) Statistical distribution of the distances d_{en} between the $N_e = 3$ electron and the $N_n = 200$ nuclear spins with randomly generated positions.

applied magnetic field is tilted with respect to the z axis, $\mathbf{B} = B(\sin\theta\hat{\mathbf{x}} + \cos\theta\hat{\mathbf{z}})$, $\langle k|s_i|k\rangle_{C_z}^\theta$ (with $k = 0, 1$) are oriented along $\mathbf{B}'_k = (B_x, 0, B_z \pm \Delta/g\mu_B)$. Eigenstates of opposite chirality are thus characterized by different orientations of the spin expectation values [see Fig. 1(b)],

$$\langle k|s_{x,i}|k\rangle_{C_z}^\theta = \sin\alpha_k/6, \quad \langle k|s_{z,i}|k\rangle_{C_z}^\theta = \cos\alpha_k/6, \quad (6)$$

where $\alpha_k = \arctan\left[\frac{\chi B \sin\theta}{B \cos\theta + (-1)^k \Delta/g\mu_B}\right] + \pi$, $0 \leq \arctan \leq \pi$, and $\chi = \pm 1$ for $\Delta \gtrless Bg\mu_B$.

If no Dzyaloshinskii-Moriya interaction is present and one exchange coupling differs from the other two, the term $H_1^{C_z}$ is replaced by $H_1^{S_{12}}$ [Eq. (3)]. For $H_e = H_0 + H_1^{S_{12}}$, the four lowest eigenstates can be labeled after the partial sum of the first two spins, rather than the spin chirality, $|S_{12}, S_z\rangle$, where $S_{12} = 0, 1$. Their expressions read $|0, +1/2\rangle = (|\uparrow\downarrow\uparrow\rangle - |\downarrow\uparrow\uparrow\rangle)/\sqrt{2}$, $|1, +1/2\rangle = (|\uparrow\downarrow\uparrow\rangle + |\downarrow\uparrow\uparrow\rangle - 2|\uparrow\uparrow\downarrow\rangle)/\sqrt{6}$, while $|S_{12}, -1/2\rangle = \sigma_x^1 \sigma_x^2 \sigma_x^3 |S_{12}, +1/2\rangle$. Choosing S_{12} as the computational DOF, one has

$$\begin{aligned} |0\rangle_{S_{12}} &= |S_{12} = 0; S_z = -1/2\rangle, \\ |1\rangle_{S_{12}} &= |S_{12} = 1; S_z = -1/2\rangle. \end{aligned}$$

As far as the spin expectation values are concerned, S_{12} represents an intermediate case between S_z and C_z . The qubit states have in fact identical values for the total spin, $\langle 0|\mathbf{S}|0\rangle_{S_{12}} = \langle 1|\mathbf{S}|1\rangle_{S_{12}}$, as C_z , but they strongly differ in terms of spin texture, as S_z [Fig. 1(a)]:

$$\langle 0|s_{z,i=1,2}|0\rangle_{S_{12}} = 0, \quad \langle 0|s_{z,3}|0\rangle_{S_{12}} = -1/2, \quad (7a)$$

$$\langle 1|s_{z,i=1,2}|1\rangle_{S_{12}} = -1/3, \quad \langle 1|s_{z,3}|1\rangle_{S_{12}} = 1/6. \quad (7b)$$

Nuclear spin and hyperfine interactions. The decoherence of the spin-cluster qubit is investigated by simulating the

coupled dynamics of electron and nuclear spins. The qubit and the nuclear environment are initialized respectively in the linear superposition $|\psi_e(0)\rangle = \frac{1}{\sqrt{2}}(|0\rangle + |1\rangle)$ and in the mixed state $\rho_n(0) = \sum_{\mathcal{I}} P_{\mathcal{I}} |\mathcal{I}\rangle \langle \mathcal{I}|$. Here, the expressions of $|0\rangle$ and $|1\rangle$ depend on H_1 , while $|\mathcal{I}\rangle = |m_1^{\mathcal{I}}, \dots, m_{N_n}^{\mathcal{I}}\rangle$ and $m_i^{\mathcal{I}}$ are the projections along the magnetic field direction of the N_n nuclear spins. In the pure-dephasing regime, each state $|\Psi_{\mathcal{I}}(0)\rangle = \frac{1}{\sqrt{2}}(|0\rangle + |1\rangle) \otimes |\mathcal{I}\rangle$ evolves into $|\Psi_{\mathcal{I}}(t)\rangle = \frac{1}{\sqrt{2}}(|0, \mathcal{I}_0\rangle + |1, \mathcal{I}_1\rangle)$, where $|\mathcal{I}_0\rangle$ ($|\mathcal{I}_1\rangle$) can be regarded as the state of the nuclear bath conditioned upon the qubit being in the $|0\rangle$ ($|1\rangle$) state. The degree of coherence in the reduced density matrix of the qubit, $\rho_e = \text{Tr}_n\{\sum_{\mathcal{I}} P_{\mathcal{I}} |\Psi_{\mathcal{I}}(t)\rangle \langle \Psi_{\mathcal{I}}(t)|\}$, is given by the so-called decoherence factor $r(t) = \sum_{\mathcal{I}} P_{\mathcal{I}} r_{\mathcal{I}}(t)$, with $r_{\mathcal{I}}(t) = \langle \mathcal{I}_1(t)|\mathcal{I}_0(t)\rangle$ and $\langle 0|\rho_e|1\rangle = r_{\mathcal{I}}/2$.

The nuclear-spin bath we consider consists of $N_n = 200$ hydrogens ($I = 1/2$), whose positions \mathbf{r}_p^n are randomly generated so as to reproduce typical values of the spin density and the electron-nuclear distances $d_{en} = |\mathbf{r}_i^e - \mathbf{r}_p^n|$, where \mathbf{r}_i^e are the positions of electron spins [Fig. 1(c)].¹⁸ The nuclear-spin Hamiltonian H_n includes Zeeman and dipole-dipole terms, $H_n = \hat{\mathbf{B}} \cdot \sum_p \omega_p \mathbf{I}_p + D_{nn} \sum_{p < q} (\mathbf{I}_p \cdot \mathbf{I}_q - 3(\mathbf{I}_p \cdot \hat{\mathbf{r}}_{pq})(\mathbf{I}_q \cdot \hat{\mathbf{r}}_{pq}))/r_{pq}^3$, where $D_{nn} = (\mu_0/4\pi)\mu_n^2\gamma_I^2$ and $\mathbf{r}_{pq} = \mathbf{r}_p^n - \mathbf{r}_q^n$. Electron and nuclear spins are coupled by dipole-dipole and contact interactions, $H_{en} = D_{en} \sum_i \sum_p [s_i \cdot \mathbf{I}_p - 3(s_i \cdot \hat{\mathbf{r}}_{ip})(\mathbf{I}_p \cdot \hat{\mathbf{r}}_{ip})]/r_{ip}^3 + \sum_i a_i s_i \cdot \mathbf{I}_{(i)}$, where $D_{en} = (\mu_0/4\pi)\mu_n \mu_e \gamma_I \gamma_e$ and $\mathbf{r}_{ip} = \mathbf{r}_i^e - \mathbf{r}_p^n$. The contact terms a_i , whose effect will be considered in the final part of this Rapid Communication, couples electron and nuclear spins belonging to the same magnetic center.

The dephasing arises from the qubit-state dependent dynamics of the nuclear bath, generated by an effective Hamiltonian \mathcal{H} . We use a two-step procedure^{19,20} to derive \mathcal{H} from the Hamiltonian $H = H_e + H_n + H_{en}$. We first replace in H the single-electron-spin operators $s_{\alpha,i}$ with their projection onto the $S = 1/2$ subspace, $s_p^\alpha \rightarrow \sum_{i,j=0}^3 \langle i|s_p^\alpha|j\rangle \sigma_{ij}$, where $\sigma_{ij} = |i\rangle\langle j|$ and $|i\rangle$ are the eigenstates of H_e . We then apply a Schrieffer-Wolff transformation to the projected Hamiltonian \mathcal{H} that removes from the Hamiltonian the terms that are off diagonal in the basis of electron-spin eigenstates $|i\rangle$,^{21,22} and finally neglect energy nonconserving terms (secular approximation). The resulting Hamiltonian reads $\mathcal{H} = \mathcal{H}^i + (|0\rangle\langle 0| - |1\rangle\langle 1|) \otimes \mathcal{H}^e$, where

$$\mathcal{H}^{\chi=i,e} = \sum_{p=1}^{N_n} \omega_p^\chi I_p^{z'} + \sum_{p \neq q} (A_{pq}^\chi I_p^{z'} I_q^{z'} + B_{pq}^\chi I_p^+ I_q^-) \quad (8)$$

and $\hat{\mathbf{z}} \equiv \mathbf{B}/B$. Two-spin terms in the intrinsic Hamiltonian \mathcal{H}^i come from dipolar interactions between the nuclei. Those in the extrinsic Hamiltonian \mathcal{H}^e are mediated by virtual transitions between eigenstates of the electron-spin Hamiltonian: They thus depend quadratically on the hyperfine couplings D_{en} , while the dependence of ω_p^e is linear. The time evolution of the nuclear states $|\mathcal{I}_k\rangle$ is computed within the pair-correlation approximation, where the nuclear dynamics is traced back to independent flip-flop transitions between pairs of nuclear spins.^{21,23,24}

Hyperfine-induced decoherence. The fastest contribution to dephasing in the spin-cluster qubit is related to

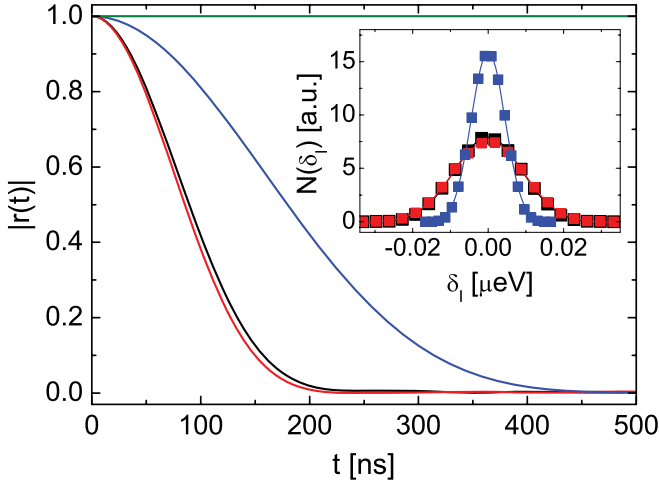


FIG. 2. (Color online) Time dependence of the decoherence factor r for the three qubit encodings: S_z (black), S_{12} (red), and C_z (green for $\theta = 0$ and blue for $\theta = \pi/8$). The curves are averaged over $N_{\mathcal{I}} = 5 \times 10^4$ randomly generated initial states $|\mathcal{I}\rangle$ of the nuclear bath. Inset: Statistical distribution (squares) of the parameter $\delta_{\mathcal{I}}$, and corresponding Gaussian fits (solid lines).

inhomogeneous broadening, and typically takes place on time scales that are much shorter than those characterizing the dynamics of the nuclear bath ($\tau_n \sim \hbar/|B_{pq}^k| \sim 10^2 \mu\text{s}$). Such a contribution results from the following renormalization of the energy gap between the states $|0\rangle$ and $|1\rangle$ induced by the hyperfine interaction: $\delta_{\mathcal{I}} = \sum_{k=0,1} (-1)^k \langle k, \mathcal{I} | \mathcal{H} | k, \mathcal{I} \rangle \simeq \sum_p \omega_p^e m_p^{\mathcal{I}}$. Being the nuclear spin bath initially in a mixture of states $|\mathcal{I}\rangle$, the decoherence factor evolves as $r(t \ll \tau_n) \simeq e^{-i(E_0 - E_1)t} \sum_{\mathcal{I}} P_{\mathcal{I}} e^{-i\delta_{\mathcal{I}} t}$, while $|\mathcal{I}_k(t \ll \tau_n)\rangle \simeq |\mathcal{I}\rangle$. In first order in H_{en} , $\delta_{\mathcal{I}}$ can be regarded as a function of the Overhauser field at the electron-spin sites,

$$\delta_{\mathcal{I}} \simeq \mu_B g \sum_i \mathbf{B}_{\text{hf}}^{\mathcal{I}}(\mathbf{r}_i^e) \cdot [\langle 0 | \mathbf{s}_i | 0 \rangle - \langle 1 | \mathbf{s}_i | 1 \rangle], \quad (9)$$

where $\mathbf{B}_{\text{hf}}^{\mathcal{I}}(\mathbf{r}_i^e) = D_{en} \sum_p m_p^{\mathcal{I}} [\hat{\mathbf{z}}' - 3(\hat{\mathbf{z}}' \cdot \hat{\mathbf{r}}_{ip}) \hat{\mathbf{r}}_{ip}] / r_{ip}^3$. In the case of the S_z qubit [see Eq. (4)], $\delta_{\mathcal{I}}^{S_z} \simeq -(\mu_B g/3) \sum_i B_{\text{hf},z}^{\mathcal{I}}(\mathbf{r}_i^e)$. The statistical distribution $N(\delta_{\mathcal{I}}^{S_z})$ is reported in the inset of Fig. 2 (black squares) for 5×10^4 initial nuclear states $|\mathcal{I}\rangle$, randomly generated from a flat probability distribution $P_{\mathcal{I}} = 1/2^{N_n}$. $N(\delta_{\mathcal{I}}^{S_z})$ is well fitted by a Gaussian function (solid line), with $\sigma_{S_z} = 9.0$ neV. Correspondingly, the decay of $|r(t)|$ (black line in Fig. 2) is approximately Gaussian, and its characteristic time scale is 10^2 ns. In the case of the S_{12} qubit, the three electron spins are no longer equivalent, and $\delta_{\mathcal{I}}^{S_{12}} \simeq -(\mu_B g/3) [2B_{\text{hf},z}^{\mathcal{I}}(\mathbf{r}_1^e) - B_{\text{hf},z}^{\mathcal{I}}(\mathbf{r}_2^e) - B_{\text{hf},z}^{\mathcal{I}}(\mathbf{r}_3^e)]$. However, the statistical distribution of $\delta_{\mathcal{I}}^{S_{12}}$ strongly resembles that of S_z (see the red squares in the figure inset, and the Gaussian fit with $\sigma_{S_{12}} = 9.4$ neV), and so does the time evolution of the decoherence factor (red curve in the main panel). In fact, since the distances d_{ee} between electron spins are larger than the smallest d_{en} [see Fig. 1(c)],¹⁸ the spatial fluctuations of the Overhauser field within the spin triangle are comparable to its average value. In spin clusters with larger d_{en}/d_{ee} ratios (not shown here), spatial fluctuations of $\mathbf{B}_{\text{hf}}(\mathbf{r})$ are relatively small.

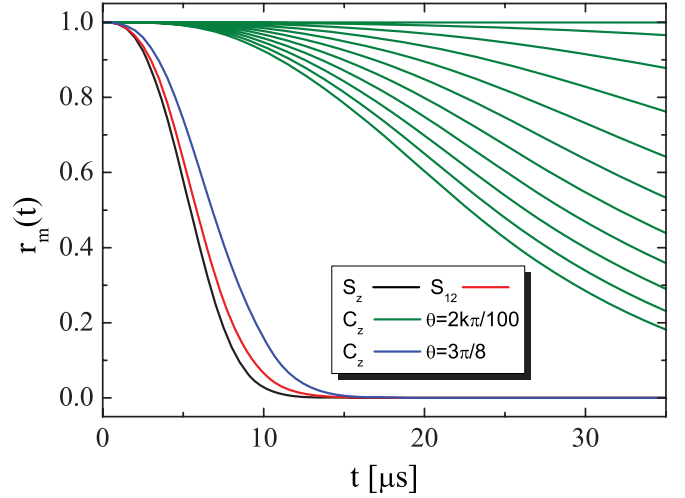


FIG. 3. (Color online) Time evolution of the decoherence factor r_m in the cases of the S_z (black) and S_{12} (red) DOFs. The case of chirality is displayed for small tilting angles $\theta = 2\pi k/100$, with k ranging from 0 (upper green curve) to 11 (lower green curves). All curves are averaged over 10^2 randomly generated initial conditions $|\mathcal{I}\rangle$; the spin Hamiltonian parameters are $\Delta = 1$ K, $B = 1$ T.

As a result, $\delta_{\mathcal{I}}^{S_{12}} \ll \delta_{\mathcal{I}}^{S_z}$, and the S_{12} qubit is less affected by inhomogeneous broadening than S_z .

In the case of the C_z qubit and for $\mathbf{B} \parallel \hat{\mathbf{z}}$, the Overhauser field does not renormalize the energy difference between the states $|0\rangle$ and $|1\rangle$ that have identical expectation values for all single-spin projections [Eqs. (5) and (9)]. The leading contribution to $\delta_{\mathcal{I}}^{C_z}$ is given by terms that are second order in the hyperfine Hamiltonian, $\delta_{\mathcal{I}}^{C_z} = \sum_{p \neq q} A_{pq}^e m_p^{\mathcal{I}} m_q^{\mathcal{I}}$, and its modulus is here five orders of magnitude smaller than that of $\delta_{\mathcal{I}}^{S_z}$ and $\delta_{\mathcal{I}}^{S_{12}}$. Correspondingly, no inhomogeneous broadening occurs in the considered time scale (green curve). For a tilted magnetic field ($\theta \neq 0$), states of opposite chirality have different expectation values $\langle \mathbf{s}_i \rangle$ [see Eq. (6)], and thus couple differently to the Overhauser field. The leading contribution to the renormalization of the energy difference reads $\delta_{\mathcal{I}}^{C_z}(\theta) \simeq (\mu_B g/6) \sum_{k=0}^1 (-1)^k (\sin \alpha_k B_{\text{hf},x'}^{\mathcal{I}} + \cos \alpha_k B_{\text{hf},z'}^{\mathcal{I}})$, where $\mathbf{x}' \perp \mathbf{z}'$ and lies in the xz plane. The statistical distribution of $\delta_{\mathcal{I}}^{C_z}(\theta = \pi/8)$ and the resulting qubit dephasing are reported in Fig. 2 ($\sigma_{C_z} = 4.5$ neV, blue curve).

The nuclear-spin dynamics contributes to decoherence by correlating electron and nuclear spins. In order to single out this contribution, we compute the function $r_m(t) = \sum_{\mathcal{I}} P_{\mathcal{I}} |r_{\mathcal{I}}(t)|$. In the case of the S_z qubit, electron-nuclear correlations result in a decay of r_m in the μs time scale (Fig. 3, black curve). The decay is induced by the interplay of the dipolar interactions between the nuclei and of the term $\sum_p \omega_p^e I_p^z$, whose expectation value gives $\delta_{\mathcal{I}}^{S_z}$. A similar time dependence for r_m is obtained in the case of the S_{12} qubit (red curve). Here, the same terms in the effective Hamiltonian \mathcal{H} dominate, and have similar expectation values, $\delta_{\mathcal{I}}^{S_z} \simeq \delta_{\mathcal{I}}^{S_{12}}$ (see the inset of Fig. 2). This quantity ($\delta_{\mathcal{I}}^{C_z}$) is about five orders of magnitude smaller for the C_z qubit, if $\mathbf{B} \parallel \hat{\mathbf{z}}$. As a result, the dynamics of the nuclear bath is largely independent on the qubit state and no appreciable decoherence takes place for $t \lesssim 10^2 \mu\text{s}$ (upper green curve): On such a time scale the $|0\rangle$ and $|1\rangle$ states

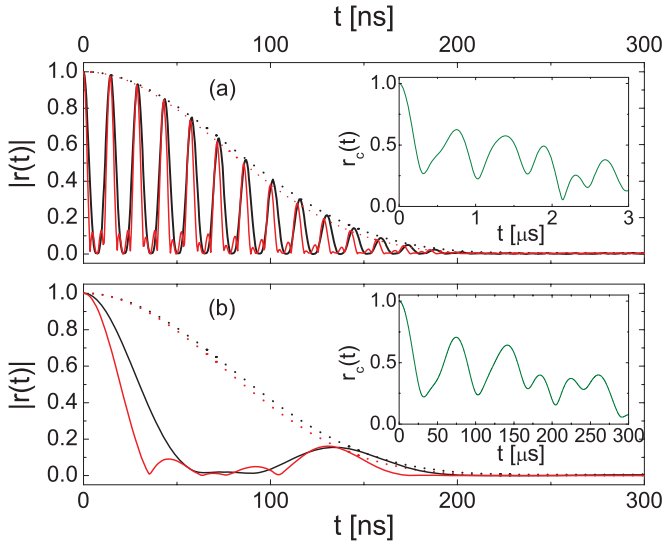


FIG. 4. (Color online) Time dependence of the decoherence factor in the presence of three additional nuclear spins ($N_n = 203$) localized at the electron-spin positions \mathbf{r}_i^e and coupled to the respective electron spins with a contact coupling (a) $a_p = 10$ mK or (b) $a_p = 1$ mK. The solid curves correspond to the cases S_z (black), S_{12} (red), and C_z (figure insets). The dotted lines represent the time dependence of r_m in the absence of the three nuclei with contact couplings.

thus define a decoherence-free subspace. However, $\delta_{\mathcal{T}}^{C_z}(\theta)$ and the decoherence rate rapidly increase for finite values of the tilting angle θ (lower green curves); for $\theta = 3\pi/8$ (blue), $r(t)$ approaches the curve corresponding to S_{12} and S_z .

We finally investigate the possible contribution to decoherence of the contact terms, resulting from the relatively strong coupling with the electron spins of few ($N_n^c \sim N_e \ll N_n$) nuclei. Here, the $N_n^c = N_e = 3$ additional nuclear spins

are localized at the electron-spin sites \mathbf{r}_i^e , and are assumed for simplicity identical to the remaining 200 nuclei. The inequivalence between the N_n^c and N_n^d nuclear spins, resulting from strong coupling of the former ones with the electron spins, warrants the factorization of the decoherence factor, $r(t) = r_c(t)r_d(t)$. The time evolution of $r_c(t)$ is reported in Fig. 4, for $a_p = 1$ and 10 mK [Figs. 4(a) and 4(b), respectively]. In the case of S_z (black curve) and S_{12} (red), r_c is responsible for the fast oscillations, while the decay is due to r_d (dotted lines). In the case of C_z , oscillations of the decoherence factor take place on a time scale which is much longer than that of S_z and S_{12} , but much shorter than the one that characterizes the contribution of the dipolar interactions (figure inset). The chirality qubit also presents a different dependence on the contact coupling constant a_i with respect to S_z and S_{12} . A comparison between the two panels shows in fact that the characteristic time scale of the oscillations in r_c is $\tau_d^c \sim \hbar/a_p$ for S_z and S_{12} , and $\tau_d^c \sim \hbar \delta_{ij}/a_p^2$ for C_z , where $\delta_{ij} \sim \min\{\Delta, g\mu_B B\}$ is the smallest difference between eigenvalues of H_e . The leading contributions of contact interaction to \mathcal{H} are thus quadratic in the hyperfine Hamiltonian for C_z , and linear for the other two DOFs.

In conclusion, we have shown that the nuclear-induced decoherence in a prototypical spin triangle strongly depends on the qubit encoding. In particular, no appreciable decoherence is found for the chirality qubit up to $10^2 \mu\text{s}$, due to the decoupling of C_z from both the total-spin orientation and the spin texture. The eigenstates of S_{12} are instead characterized by decoherence times comparable to those of the total-spin projection S_z , unless the distance between electron spins is strongly reduced with respect to the size of the nuclear bath.

We acknowledge financial support by PRIN of the Italian MIUR, by the Swiss NF, and by FP7-ICT project “ELFOS.”

¹D. Gatteschi, R. Sessoli, and J. Villain, *Molecular Nanomagnets* (Oxford University Press, Oxford, UK, 2007).

²See, e.g., C. Klocffel and D. Loss, arXiv:1204.5917.

³F. Meier, J. Levy, and D. Loss, *Phys. Rev. Lett.* **90**, 047901 (2003).

⁴F. Troiani, A. Ghirri, M. Affronte, S. Carretta, P. Santini, G. Amoretti, S. Piligkos, G. Timco, and R. E. P. Winpenny, *Phys. Rev. Lett.* **94**, 207208 (2005).

⁵J. Lehmann, A. Gaita-Ariño, E. Coronado, and D. Loss, *Nat. Nanotechnol.* **2**, 312 (2007).

⁶M. Trif, F. Troiani, D. Stepanenko, and D. Loss, *Phys. Rev. Lett.* **101**, 217201 (2008).

⁷M. Trif, F. Troiani, D. Stepanenko, and D. Loss, *Phys. Rev. B* **82**, 045429 (2010).

⁸M. F. Islam, J. F. Nossa, C. M. Canali, and M. Pederson, *Phys. Rev. B* **82**, 155446 (2010).

⁹N. Baadji, M. Piacenza, T. Tugsuz, F. Della Sala, G. Maruccio, and S. Sanvito, *Nat. Mater.* **8**, 813 (2009).

¹⁰A. Ardavan, O. Rival, J. J. L. Morton, S. J. Blundell, A. M. Tyryshkin, G. A. Timco, and R. E. P. Winpenny, *Phys. Rev. Lett.* **98**, 057201 (2007).

¹¹S. Bertaina, S. Gambarelli, T. Mitra, B. Tsukerblat, A. Müller, and B. Barbara, *Nature (London)* **453**, 203 (2008).

¹²C. Schlegel, J. van Slageren, M. Manoli, E. K. Brechin, and M. Dressel, *Phys. Rev. Lett.* **101**, 147203 (2008).

¹³K.-Y. Choi, Y. H. Matsuda, H. Nojiri, U. Kortz, F. Hussain, A. C. Stowe, C. Ramsey, and N. S. Dalal, *Phys. Rev. Lett.* **96**, 107202 (2006).

¹⁴C. Schlegel, J. van Slageren, G. Timco, R. E. P. Winpenny, and M. Dressel, *Phys. Rev. B* **83**, 134407 (2011).

¹⁵P. Zanardi, and M. Rasetti, *Phys. Rev. Lett.* **79**, 3306 (1997).

¹⁶L.-M. Duan, and G. C. Guo, *Phys. Rev. Lett.* **79**, 1953 (1997).

¹⁷D.-A. Lidar, I. L. Chuang, and K. B. Whaley, *Phys. Rev. Lett.* **81**, 2594 (1998).

¹⁸The distance between any two electron spins is 5 Å. The nuclei are distributed in a sphere of radius $R = 10$ Å, with the constraints $|\mathbf{r}_i^e - \mathbf{r}_j^e| \geq 1.5$ Å and $|\mathbf{r}_i^e - \mathbf{r}_j^e| \geq 3$ Å.

¹⁹A. Szallas and F. Troiani, *Phys. Rev. B* **82**, 224409 (2010).

²⁰F. Troiani, V. Bellini, and M. Affronte, *Phys. Rev. B* **77**, 054428 (2008).

- ²¹W. Yao, R.-B. Liu, and L. J. Sham, *Phys. Rev. B* **74**, 195301 (2006).
- ²²W. A. Coish, J. Fischer, and D. Loss, *Phys. Rev. B* **77**, 125329 (2008).

- ²³W. M. Witzel, R. de Sousa, and S. Das Sarma, *Phys. Rev. B* **72**, 161306(R) (2005).
- ²⁴W. Yang and R.-B. Liu, *Phys. Rev. B* **78**, 085315 (2008).